Case Studies in Construction Materials 23 (2025) e05145

Contents lists available at ScienceDirect

Case Studies in Construction Materials

journal homepage: www.elsevier.com/locate/cscm

High-dosage carbide slag-based cementitious material: Workability, mechanical strength, and carbonation behavior with the performance enhancement

Yulong Zheng [a,*], Chang Liu [a], Jingquan Wang [a,*], Haozhe Pan [b,c,**], Xingpei Yan [a,b], Stuart T. Wagland [c], Guiyu Zhang [a], Liang Cheng [d]

[a] Faculty of Civil Engineering and Mechanics, Jiangsu University, Zhenjiang, Jiangsu 212013, China
[b] Faculty of Materials and Civil Engineering, Jiangsu University Jingjiang College, Zhenjiang, Jiangsu 212028, China
[c] Faculty of Engineering and Applied Sciences, Cranfield University, Cranfield MK43 0AL, UK
[d] School of Environment and Safety Engineering, Jiangsu University, Zhenjiang, Jiangsu 212013, China

ARTICLE INFO

Keywords:
Carbide slag
Working and mechanical properties
Carbon capture
Hydration mechanism
Solid wastes

ABSTRACT

Cement production generates substantial carbon emissions, necessitating low-carbon alternatives. This study utilized high-dosage carbide slag, a solid waste byproduct of the acetylene industry, to prepare an environmentally friendly and low carbon cementitious materials-CFG (Carbide slag-Fly ash-GGBS system). To investigate the comprehensive performance of CFG, the effects of different dosages of carbide slag (CS, 10 %-70 %) and silica fume (SF, 0 % or 10 %), as well as the CO_2 capture capacity, were investigated. The environmental assessment was also carried out by using the Life Cycle Assessment (LCA) method. The flexural and compressive strengths of CFG with 10 % CS reached 7.7 and 29.2 MPa, respectively, at 28 days. It is clear from the micro-analysis that the CS mainly acts as an alkaline stimulant in the cementitious system and can effectively activate FA and GGBS to produce gels. Excessive CS in the system caused $Ca(OH)_2$ accumulation, which negatively affected the system's strength. This can be remedied by adding SF and carbonization. In particular, after carbonation, the compressive strength of specimens with 30 % CS increased by 32.7 % from 31.1 MPa to 35.7 MPa and with 70 % CS increase by 80 % from 11 MPa to 19.8 MPa, demonstrating excellent carbon sequestration enhancement properties. The environmental evaluation of the system using LCA shows a substantial suppression of CO_2 emissions and energy consumption, with 89.12 % and 80.35 % reduction, respectively, compared with ordinary Portland cement. Therefore, along with the massive consumption of solid waste, CFG is an environmentally friendly material with the potential to replace conventional cement.

1. Introduction

Carbide slag (CS) is a solid waste byproduct primarily composed of calcium hydroxide, produced during the hydrolysis of calcium carbide to produce acetylene gas. Statistics show that about 150–190 million tons of CS globally are produced annually [1,2]. Approximately 56 million tons of CS are mainly produced annually in China [3,4], while less than 40 % is effectively utilized [5,6]. The

* Corresponding authors.
** Corresponding author at: Faculty of Materials and Civil Engineering, Jiangsu University Jingjiang College, Zhenjiang, Jiangsu 212028, China.
E-mail addresses: zylcivil@ujs.edu.cn (Y. Zheng), wangjingquan@seu.edu.cn (J. Wang), hpanaa@connect.ust.hk (H. Pan).

https://doi.org/10.1016/j.cscm.2025.e05145
Received 29 May 2025; Received in revised form 17 July 2025; Accepted 4 August 2025
Available online 5 August 2025
2214-5095/© 2025 The Authors. Published by Elsevier Ltd. This is an open access article under the CC BY-NC-ND license (http://creativecommons.org/licenses/by-nc-nd/4.0/).

substantial accumulation of this alkaline CS waste occupies significant land resources, resulting in severe air, water, and soil pollution [7,8], and poses a significant challenge to sustainable production processes. As a result, the treatment and utilization of CS have essential value for environmental sustainability and have attracted considerable research interest.

Several strategies have been proposed to expand the recycling of CS. Due to its high $Ca(OH)_2$ content, CS is often employed to treat acidic gases, such as converting SO_2 in flue gas to achieve desulfurization [9]. It can also be a substitute for quicklime as a neutralizing agent in treating acidic wastewater or wastewater containing toxic elements [10,11]. As a calcium-rich material, CS has been studied to synthesize high-value chemicals like light/nano calcium carbonate and calcium format [12,13]. However, the market demand for the utilization methods mentioned above is relatively small, and the consumption scale of waste CS is limited, which cannot significantly change the corresponding environmental issues [14].

Further, cement production is pivotal in construction, marked by substantial output and significant environmental impact. The industry's high consumption of resources and extensive pollution levels are concerning [15–17]. Each ton of cement is estimated to produce approximately 0.8 tons of CO_2 emissions, contributing significantly to atmospheric CO_2 levels [18]. Recent studies have emphasized the potential of calcium-rich industrial wastes like fly ash (FA), ground granulated blast furnace slag (GGBS), and CS to serve as alternative binder materials, addressing environmental concerns [19–21]. Utilizing these industrial wastes to produce low-carbon cementitious materials could markedly improve the recycling rate of CS, reduce the cement industry's reliance on natural resources, and alleviate environmental pollution.

Currently, research on the use of CS to produce cementitious materials has received increasing attention. Qi et al. [22] conducted mechanical tests on a cementitious material consisting of CS and GGBS and found that it could reach a strength of about 15.29 MPa at 28 days. Similarly, Li et al. [23] found that the compressive strength of the CS-GGBS system was about 21 MPa after 28 days when the CS content was 5 %. The authors also discovered that the system's strength decreased as the CS content increased. Through experiments, Feng et al. [24] found that the increase in the dosage of CS could increase the number of hydration products in the CS-GGBS cementitious system. In addition to the combination of CS and GGBS, Dueramae et al. [25] used CS and FA to prepare cementitious materials, with a mass ratio of 3:7. The results showed that the system's compressive strength after 28 days was about 22.3 MPa. Microscopic analysis revealed that the FA particles did not react completely, failing to form sufficient effective gel products. Namarak et al. [26] also synthesized cementitious materials from CS and FA based on the same mass mix ratio (3:7) and found that the compressive strength of the system at 28 days was about 19 MPa. Phongthorn et al. [27] reported the law of strength variation in the CS-FA cementitious system with $CaO/(SiO_2+Al_2O_3)$ ratios in the range of 0.9–1.7. The results indicated that the strength of the system first increased and then decreased with the increase of CS dosage and that the incorporation of CS had a certain facilitating effect on the pozzolanic reaction of FA. In addition, some researchers have made binary cementitious materials by mixing CS with materials such as rice husk ash and bagasse. However, inferior to the CS-GGBS and CS-FA systems, the compressive strength after 28 days was relatively low (less than 15 MPa) [28,29].

Previous studies have shown that the binary cementitious system consisting of CS, GGBS, or FA can have a certain degree of mechanical performance, which is better than that of other binary systems. This may be due to the fact that GGBS and FA contain mainly amorphous silica-alumina phases, as well as partially crystalline phases, which are potentially volcanic-ash-active and high in Si and Al, and can be hydrated to produce relatively large amounts of gellant materials under certain conditions [30]. However, it must also be pointed out that the compressive strength of both the CS-GGBS system and the CS-FA system is still some distance away from that of conventional cement. This may be due to the limited amount of active SiO_2 and Al_2O_3 provided by a single GGBS or FA, which is insufficient to generate enough gel material through subsequent reactions, resulting in an insufficiently dense system interior. Therefore, existing studies mostly focus on binary systems, establishing a ternary cementitious system (CFG) based on CS, GGBS, and FA with increased silica-aluminum content in the components might enhance the later hydration products and potentially increase the overall strength of the cementitious system. In addition, although some studies have shown that CS can promote the hydration reaction of GGBS and FA, the specific mechanism is unclear. The dosage of CS in the cementitious system in the existing studies is relatively low (5 %-25 %), so further studies are needed to analyze the effect of different dosages of CS on the system and the specific mechanism of action. Additionally, many studies have shown that silica fume (SF) can improve the performance of cement-based materials [31,32] through synergistic effects, but its potential positive impact on low-carbon cementitious systems still needs verification. Furthermore, CS is rich in $Ca(OH)_2$, which may have carbon sequestration potential, as confirmed by previous studies [33–35]. However, the interaction mechanism between CS and CO_2 within cementitious systems has been explored to a limited extent.

This study explores the feasibility of preparing low-carbon cementitious systems using a combination of CS, FA, GGBS, and SF. To facilitate the large-scale application of solid waste, the effect of CS doped at levels ranging from 10 % to 70 % is systematically investigated. Specifically, the workability and strength development of the CFG system at 3, 7, and 28 days are analyzed, and microscopic mechanism analysis is incorporated to determine the optimal mix proportions. Due to the possibility of excess alkaline calcium hydroxide in the CFG with high-dosage CS, carbonation tests are conducted to assess the carbon capture and performance enhancement capabilities of CFG. Additionally, since solid waste is used to replace cement, a Life Cycle Assessment (LCA) is employed to evaluate the energy-saving and emission-reduction effects of CFG throughout the preparation process, thereby demonstrating its comparison with ordinary Portland cement (OPC) in terms of carbon emissions and energy consumption. Therefore, this study is considered to propose an innovative cementitious material system.

Table 1
Chemical composition of the raw materials (wt%).

Materials	CaO	SiO_2	Al_2O_3	SO_3	Fe_2O_3	MgO	Na_2O	K_2O	TiO_2	LOI
CS	81.09	11.00	2.57	1.57	0	1.28	0.96	0.39	0.20	0.24
FA	5.22	48.56	29.67	1.73	6.32	1.82	0.92	1.17	1.13	3.46
GGBS	40.20	30.05	14.28	2.81	0.43	8.61	0.43	0.52	1.96	0.71
SF	0.10	96.23	0.31	-	0.07	0.11	0.97	-	-	2.6

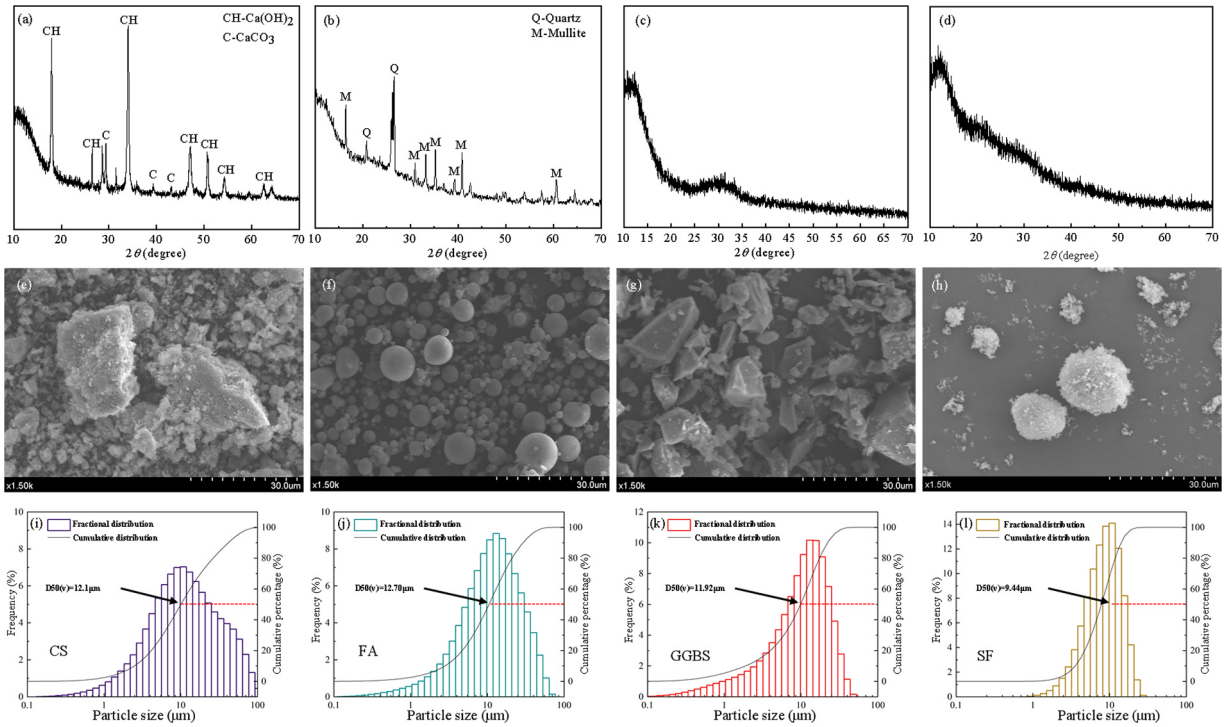


Fig. 1. XRD, SEM and PSD analysis of raw materials: (a) XRD of CS; (b) XRD of FA; (c) XRD of GGBS; (d)XRD of SF; (e) SEM of CS; (f) SEM of FA; (g) SEM of GGBS; (h) SEM of SF;(i) PSD of CS; (j) PSD of FA; (k) PSD of GGBS; (l) PSD of SF.

2. Materials and methods

2.1. Raw materials

The materials used to prepare the CFG system in this experiment include CS, FA, GGBS, SF, standard sand, and water. CS, provided by Nanjing Jinjiali New Materials Technology Co., Ltd., was initially in slurry form and dried at 105°C. FA supplied by Henan Borun Casting Materials Co., Ltd. was Grade 1 low-calcium FA. GGBS, sourced from Henan Borun Casting Materials Co., Ltd., was S95 grade slag. SF was obtained from Gongyi Hengnuo Filter Material Co., Ltd. The chemical compositions determined by X-ray fluorescence (XRF) analysis are shown in Table 1. It can be speculated that FA and GGBS may provide silicon and aluminum for the hydration reaction, while $Ca(OH)_2$ (81.09 wt%) in CS may provide a high pH environment to promote the dissociation of Si-O-Al bonds in FA/GGBS. Further, the high silica content in SF may undergo Si-O-Si bond cleavage in the alkaline medium, and then reacts with Ca^{2+} ions from $Ca(OH)_2$ to form calcium silicate hydrate (C-S-H) and calcium aluminosilicate hydrate (C-A-S-H) gels.

The mineral phases and microstructures of the raw materials were analyzed using X-ray diffraction (XRD) and scanning electron microscopy (SEM), as shown in Fig. 1. The primary mineral component of CS was $Ca(OH)_2$, characterized by a plate-like morphology with a rough surface and a large specific surface area [36,37]. FA exhibited significant amounts of quartz and mullite, primarily in spherical structures. GGBS displayed a distinct amorphous peak, indicating a high content of amorphous SiO_2 and Al_2O_3, with microstructures predominantly composed of irregular plate-like particles. SF showed peaks in the 10–20° range, suggesting a substantial amount of active SiO_2, with microstructures mainly consisting of spherical particles. The particle size distribution (PSD) of each material was measured using a NKT5200-H laser particle analyzer (Shandong Nikete Instrument Co., Ltd.), as shown in Fig. 1(i) to (l).

Table 2
Mix proportions of mortar samples.

Mix No.	CS(%)	FA(%)	GGBS(%)	Sand(%)	SF(%)	Water (%)
0CS*	0	33.3	66.7	300	-	50
5CS*	5	31.7	63.3	300	-	50
10CS*	10	30	60	300	-	50
20CS	20	26.7	53.3	300	-	50
30CS*	30	23.3	46.7	300	-	50
40CS	40	20	40	300	-	50
50CS*	50	16.7	33.3	300	-	50
60CS	60	16.7	33.3	300	-	50
70CS*	70	13.3	26.7	300	-	50
30CS10SF	30	20	40	300	10	50

Note: The group 30CS10SF indicates 30 % CS and 10 % SF dosing, and those with * are characteristic proportioning groups, for which both flexural and compressive strengths were tested, while the remaining groups were only tested for compressive strength.

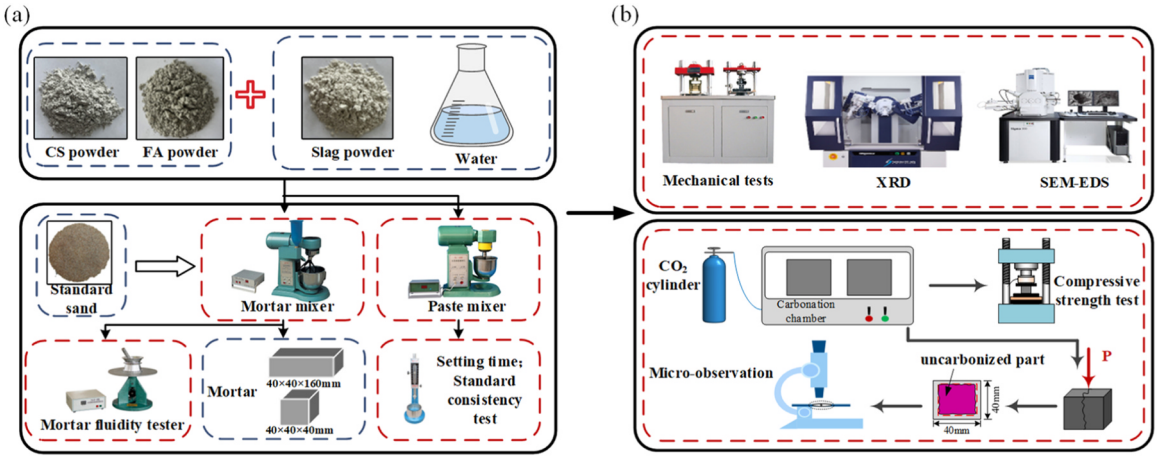


Fig. 2. Preparation and test flow chart of CFG cementitious material:(a) preparation of specimens and working performance tests; (b) mechanical property tests, microanalysis, and carbonization tests.

2.2. Mix proportions and preparation of CFG

2.2.1. Mix proportions

Based on previous experimental studies and literature reviews, the optimal mixing ratio of FA to GGBS was 1:2 [38,39]. A constant water-to-binder mass ratio of 0.5 was used to prepare the mortar samples, with a binder-to-aggregate ratio of 1:3. Various CS dosages (0 %, 5 %, 10 %, 20 %, 30 %, 40 %, 50 %, 60 %, and 70 %) were incorporated into the CFG mixtures to investigate the effects of different CS contents on the performance of the CFG system. In addition, according to studies related to cementitious materials [40], 10 % silica fume (SF) was added to the 30 % CS mixture to verify the possible improvement effect of SF on the system. The mixture design is detailed in Table 2.

2.2.2. Sample preparation

According to GB/T 17671–2021, all proportioned dry materials were uniformly mixed, and water and standard sand were thoroughly stirred to form the cement mortar. The slurry was poured into standard moulds and de-moulded after 24 h in a standard curing chamber. Standard triplet mortar specimens of 40 mm × 40 mm × 160 mm were prepared for determining the flexural and compressive strengths of the characteristic mix proportions, while standard triplet mortar specimens of 40 mm × 40 mm × 40 mm were prepared for compressive strength of the remaining mix proportions and carbonation tests. The standard curing chamber conditions were maintained at a temperature of 20 ± 2°C and a relative humidity of 95 ± 5 %. The detailed preparation process and testing methods are illustrated in Fig. 2.

2.3. Experimental methods

2.3.1. The water requirement for normal consistency and setting time

The Vicat apparatus measured the water required for the cementitious materials to achieve normal consistency and the setting time according to the guidelines specified in GB/T 1346–2011. The initial setting time is recorded when the needle penetrates to a depth of

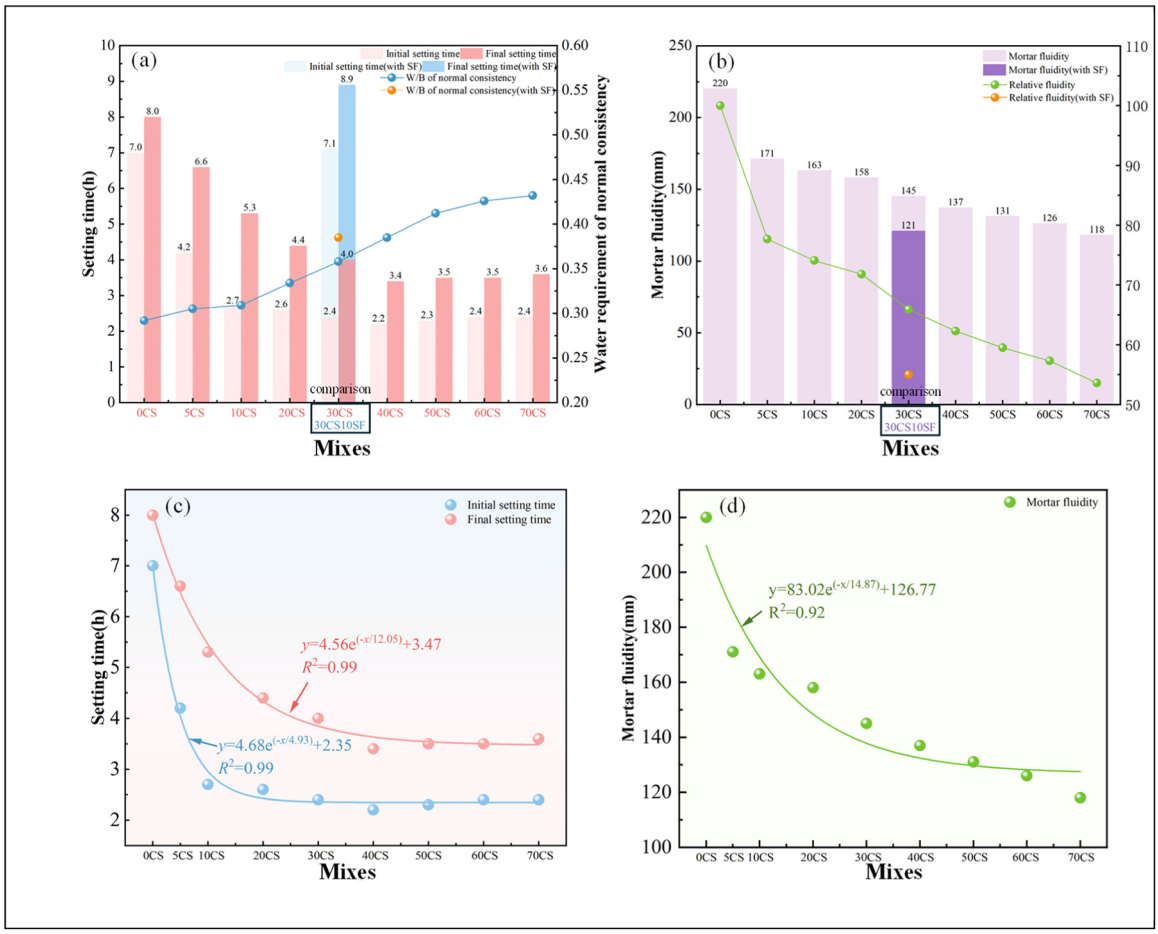


Fig. 3. The workability of CFG: (a) setting time and water requirement of standard consistency; (b) mortar fluidity; (c) fitting relationship of setting time; (d) fitting relationship of mortar fluidity.

5 mm, and the final setting time is determined when the needle no longer leaves a visible mark. The jumping table method determined the fluidity under the standard GB/T 2419–2005. The flow table was lifted and released 25 times, and the spread diameter of the paste was measured to assess the flowability, reported as the average of three measurements.

2.3.2. Flexural and compressive strength

A three-point flexural strength test was conducted at 3, 7, and 28 days of curing, following the standard GB/T 17671–2021. The specimens were tested using a universal testing machine (DY-208JC) at a constant loading speed of 50 N/s ± 10 N/s. The reported results are the averages of three specimens. According to the standard GB/T 17671–2021, the samples were tested by a fully automatic pressure testing machine (DY-208JC) for compressive strength at 3,7 and 28 days of curing. The applied loading rate was 2400 N/s ± 200 N/s. Triplicate samples were tested for each group, and the average values are reported.

2.3.3. Microstructure and composition analysis

Cement paste specimen were prepared and subjected to pressure damage. Samples were taken from the center of the crushed fracture surface and immersed in absolute ethanol to halt hydration for XRD, SEM analyses. Before testing, the specimens were dried in an oven at 60°C until a constant weight was achieved, then ground to pass through a 100-mesh sieve. The phase composition at different curing ages was analyzed using a BRUKER D8 ADVANCE XRD, scanning the samples at a 5°/min speed in the 10–70° range. The SEM-EDS analysis was conducted using a Hitachi S-3400N scanning electron microscope equipped with an energy dispersive X-ray spectrometer (EDS). The samples were gold sputter-coated to improve conductivity. Both secondary electron (SE) and backscattered electron (BSE) images were taken for morphological and compositional analysis. The measurements were performed under a high vacuum mode at an accelerating voltage of 20 kV, to observe the microstructure, analyzing the response mechanisms of the microstructural products, gels, and their distribution changes. EDS was used to determine the elemental composition, examining the synergistic and competitive mechanisms of the materials during the setting and hardening process.

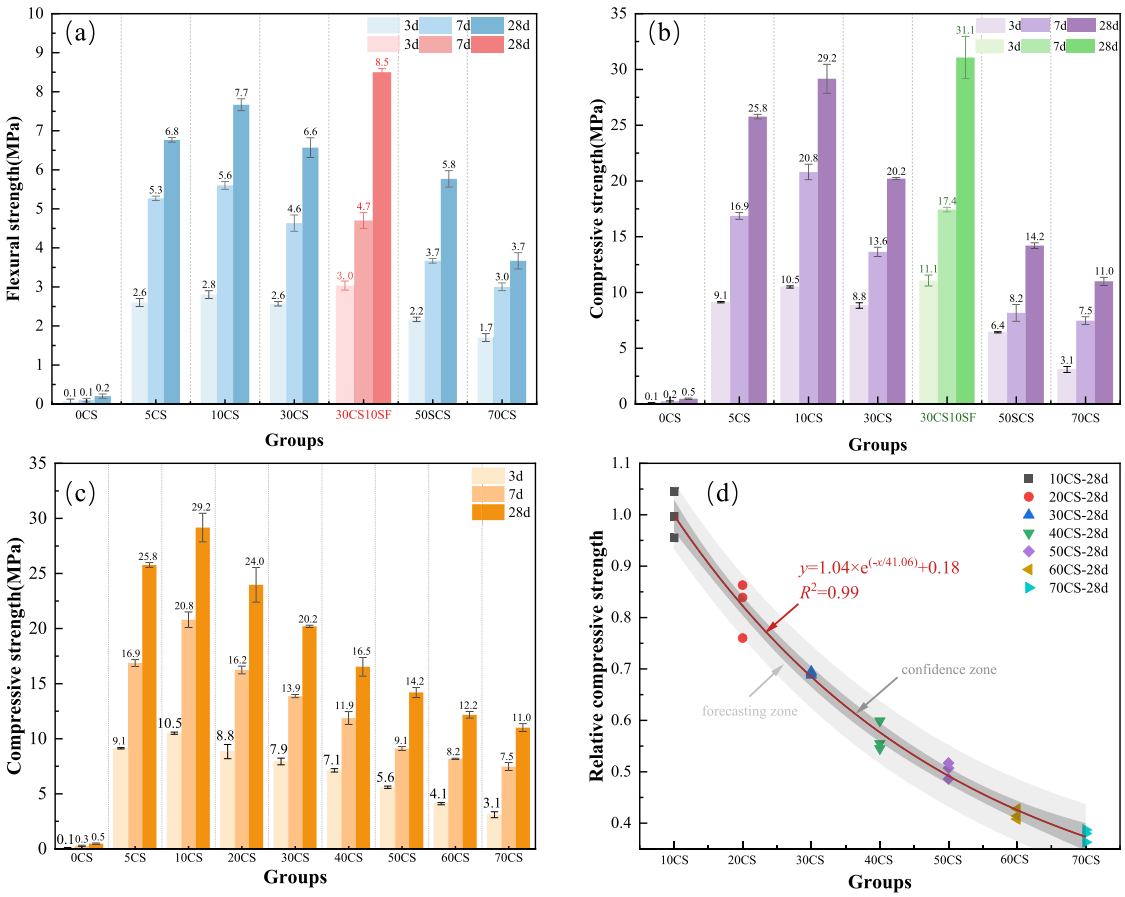


Fig. 4. Mechanical properties of CFG under different curing ages and CS dosages: (a) flexural strength of characteristic mixes; (b) compressive strength of characteristic mixes; (c) compressive strength of all mixes; (d) fitting relationship between compressive strength and CS dosage.

2.3.4. CO_2 sequestration

The carbonation test followed the standard procedure [41] using mortar specimens (40 mm*40 mm*40 mm) and a CCB-70 carbonation chamber. After standard curing for 28 days (20 ± 2℃ and 95 ± 5 % relative humidity), the specimens were dried in an external environment for 48 h before being placed in the carbonation chamber. The distance between the specimens was kept at no less than 50 mm. The chamber was then sealed, and the CO_2 flow rate was gradually adjusted to maintain a concentration of 20 ± 3 %, with humidity at 70 ± 5 % and temperature at 20 ± 2°C. As shown in Fig. 2(b), after 28 days of carbonation, compressive tests were first conducted, followed by measurements of the carbonization depth on the fracture surface. Finally, samples were taken from the fracture surface, ground, and sieved for microscopic analysis.

3. Results and discussion

3.1. The workability of CFG

To verify the practical application performance of the CFG system, its workability was first tested. The variation trends of water required for a standard consistency, the setting times, and the fluidity under different CS dosages are presented in Fig. 3.

From Fig. 3(a), it can be seen that as the proportion of CS increased, the water demand for standard consistency also rose. On the contrary, from Fig. 3(b), the data indicate that the flowability of the system decreased as the amount of CS increased. As shown in Fig. 1 (i), the particle size of CS is mostly around 12.1 μm, so it has a relatively large specific surface area. These changes are primarily due to the large specific surface area and loose, porous, and plate-like structure of the CS (as shown in Fig. 1(e)), which enhances its water absorption capacity and the friction with the cementitious components. Consequently, more water is required to achieve consistency, and the system's fluidity decreases at the same water content [29]. Further, from both Fig. 3(a) and (c), it can be seen that the setting time showed a downward trend before 10CS (mixed with 10 % CS, 30 % FA and 60 % GGBS) and then gradually stabilized. The initial setting time of CFG ranged from 2.4 to 7.1 h, and the final setting time ranged from 3.4 to 8.9 h, which generally satisfies the requirements of ordinary Portland cement (OPC) (GB/T 2419–2005, initial setting time greater than 0.75 h, final setting times less than

6.5 h). In the 0CS mix, the observed semi-rigid state after approximately 7 h is likely due to superficial stiffening caused by surface moisture loss, rather than true setting or hydration. As FA and GGBS do not exhibit self-cementitious properties without an activator like CS, no significant strength development is expected (refer to subsequent Fig. 4). Compared to 0CS, the initial and final setting times of 10CS were reduced by 33.8 % and 61.4 %, respectively, which indicates that CS may participate in the reaction of the cementing system as an activator [42,43]. This is attributed to the fact that the main component of CS is $Ca(OH)_2$, which can increase the pH value in the pore solution when dissolved in water. Thus, the addition of CS provides an alkaline environment that accelerates the hydration reaction and promotes the formation of hydration products, such as calcium silicate hydrate (C-S-H) and calcium aluminate hydrate (C-A-S-H), which are crucial for the development of strength in Cementitious materials. Additionally, calcium ions in CS provide more nucleation sites for hydration reactions, facilitating the aggregation of hydration products [44–46].

Further, from Fig. 3(a), it can be known that when 10 % silica fume was added to the 30CS system, i.e. for the 30CS10SF (mixed with 30 % CS, 20 % FA, 40 % GGBS, and 10 % SF) group, the water required for the paste to reach standard consistency had a slight increase from 0.355 to 0.385. Moreover, as shown in Fig. 3(b), the flowability decreased to 121 mm, equivalent to 83.4 % of the 30CS group. As shown in Fig. 1(l), these variations are probably attributed to the fine particle size of silica fume, which has an average size of 9.44 μm. Therefore, it has a higher water binding capacity, significantly increasing the water demand [47]. Compared with 30CS, the initial and final setting times of 30CS10SF were extended to 7.1 and 8.9 h, respectively, with increases of 195.8 % and 122.5 %. This is because the silicate phase in spherical silica powder particles exhibits lower hydration reactivity, making it more challenging to participate in the hydration reaction during the initial curing period. Therefore, due to the fact that the silicate phase in SF has low reactivity, the hydration process is delayed, forming fewer hydration products during the initial curing period [48].

Multiple candidate models were evaluated in this study, including linear, logarithmic, and single exponential functions, for data fitting. The highest R^2 values were achieved by the single exponential function, indicating optimal data fitting performance. Consequently, the exponential function was used for describing the relationship between CS dosage and material performance characteristics. Eqs. (1) and (2) below show the specific fitting formulas, with the R^2 of 0.99. It is found that the setting time of the paste is highly negatively correlated with the content of CS.

$$Inital = 4.68\exp^{(-CS(\%)/4.93)} + 2.35; R^2 = 0.99 \tag{1}$$

$$Final = 4.56\exp^{(-CS(\%)/12.05)} + 3.47; R^2 = 0.99 \tag{2}$$

Where CS (%) represents mass percentages of CS in the system; Initial/Final. represents the initial and final setting time of mortar with different dosages of CS, h.

In addition, the fitting curves of mortar flowability data are shown in Fig. 3(d), with the specific fitting formula shown in Eq. (3). It can be concluded that the flowability of mortar is also highly negatively correlated with the dosage of CS.

$$Fluidity = 83.02\exp^{(-CS(\%)/14.87)} + 126.77; R^2 = 0.92 \tag{3}$$

In which Fluidity. represents the flowability of mortar with different dosages of CS, mm.

3.2. Mechanical properties of CFG

Tests for flexural and compressive strengths were conducted to evaluate the mechanical properties of the CFG system. The test results at 3, 7, and 28 days are shown in Fig. 4(a) and(b), respectively. For groups without adding silica fume, it was observed that with increased CS content, both flexural and compressive strengths initially increased and then decreased. The maximum strengths were achieved at a CS content of 10 %, with 28-day flexural and compressive strengths of approximately 7.7 MPa and 29.2 MPa, respectively. Further, as detailed in the following carbonation section, the compressive strength of the optimal composition system reached 35.7 MPa. These values are comparable to those of Ordinary Portland cement (OPC) with strength grade 32.5 (specified strength as between 32.5 and 42.5 MPa based on GB 175–2007) and significantly higher than the strengths of the system without CS (0CS group), which were 0.2 MPa and 0.5 MPa, respectively. This trend may be attributed to the limited alkalinity provided by the hydrolysis of GGBS, which only partially promotes the pozzolanic reaction of FA, resulting in low mechanical strength. The introduction of CS might provide more OH^-, which could further promote the hydration reaction of GGBS and FA, increase the gel product, and thereby significantly improve the system strength [49].

As the CS content increased from 10 % to 70 %, a gradual decrease in the mechanical strength of the CFG system was observed, with the 28-day flexural and compressive strengths for the 70CS group decreasing to 3.7 MPa and 11 MPa, respectively, which were 51.9 % and 62.3 % lower compared to the 10CS group. As detailed in the subsequent micro-analysis section, this reduction in strength might be attributed to the excessive residual $Ca(OH)_2$ in the system, which could weaken the interlayer bonding and prevent the formation of a dense structure, thus reducing the overall strength [50]. It is also possible that the reduction of FA and GGBS, which are important raw materials for the hydration reaction, has led to a decrease in performance. Additionally, by adding silica fume to the CFG system, the 28-day flexural and compressive strengths of the 30CS10SF group were 8.5 MPa and 31.1 MPa, respectively, which were approximately 28.8 % and 54 % higher than those of the 30CS. This improvement is probably attributed to the volcanic ash effect induced by SF, which could produce additional gelatinous material that fills and optimizes the pore structure of the mortar [51].

To further explore the correlation between compressive strength and CS content beyond 10 % on the mechanical properties with excess amounts of CS, the compressive strength and its relationship under each CS dosage are listed as the representative in Fig. 4(c) and (d). It is found that the compressive strength is highly negatively correlated with the amount of CS for dosages higher than 10 %,

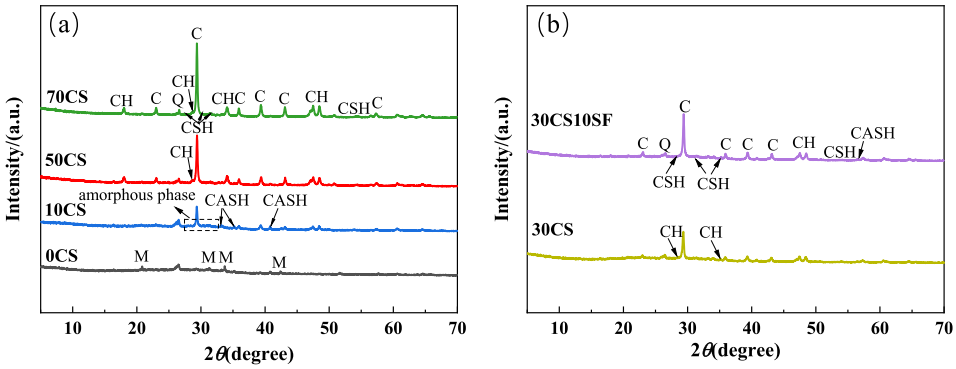


Fig. 5. XRD results of the CFG at 28d: (a) effect of different CS dosages; (b) effect of SF dosage, **Note:** M: mullite; Q: quartz; C: calcite; CASH: calcium aluminate silicate hydrates; CSH: calcium silicate hydrates; CH: calcium hydroxide.

and the specific fitting formula is shown in Eq. (4).The fitting curve is based on the 28-day compressive strength data of all mix proportions.

$$Com. = 1.04\exp^{(-CS(\%)/41.06)} + 0.18; R^2 = 0.99 \quad (4)$$

Where Com. represents the compressive strength of mortar with different dosages of CS in MPa.

3.3. Phase analysis of hydration products

The XRD patterns of various samples after 28 days of curing are presented in Fig. 5. The main crystalline phases in the CFG system included mullite (M), quartz (Q), calcite (C), calcium aluminate silicate hydrates (C-A-S-H), calcium silicate hydrates (C-S-H), calcium hydroxide (CH). The crystalline mullite phase, primarily derived from FA, was mainly represented in the cementitious system without CS. Compared with other groups (with CS), even though GGBS releases a small amount of OH^- during hydration, part of the FA may remain unreacted in the 0CS group, which might indicate that the OH^- released by the hydration of GGBS alone is insufficient to fully hydrate the FA-GGBS system. This resulted in the 0CS group not developing strength, aligning with the weaker mechanical performance test results [52]. As the CS content of the samples gradually increased (from 10 % to 70 %), a more distinct calcite phase can be observed, which could be attributed to the presence of inert $CaCO_3$, probably brought in from CS raw materials (refer to the XRD results in Fig. 1(a)). Meanwhile, a broad peak of the amorphous phase was observed with the increase of CS dosage in Fig. 5(a), characteristic of C-S-H and C-A-S-H gels [53,54].This may indicate that the addition of CS provides an alkaline environment suitable for the hydration reactions, supplies more Ca^{2+}, and increases nucleation sites, forming additional gel products [55]. The diffraction peaks of $Ca(OH)_2$ were not prominent as the CS content increased from 0 % to 10 %, suggesting almost full involvement of CS in the hydration reaction, and part of CS might be converted by the carbonization reaction. FA and GGBS consumed the $Ca(OH)_2$ from CS, enhancing the system's densification, consistent with those mentioned above, and increased compressive strength [56].

More calcite and $Ca(OH)_2$ phases were observed in CFG samples with a CS content greater than 10 %. This may be due to the increase in unreacted CS raw material, which also increases its $CaCO_3$ content caused by carbonization. This further highlights the advantages of the CFG system in long-term carbon dioxide capture. On the other hand, it can be observed from Fig. 5(a) that the diffraction peaks of $Ca(OH)_2$ were significantly increased in the 70CS sample compared to the 10CS. This may also indicate that the excess $Ca(OH)_2$ in the CFG with high CS content does not participate in further hydration reactions but only acts as a filler. As previously analyzed, the accumulation of plate-like $Ca(OH)_2$ leads to a gradual decrease in the system's compactness, which is consistent with the deterioration of the mechanical tests. The detailed mechanism and microscopic analysis will be further discussed in the following section.

Furthermore, as can be seen from Fig. 5(b), compared with the 30CS sample, the 30CS10SF sample revealed a gradual decrease in the intensity of diffraction peaks at approximately 41° 2θ angles, indicating a reduction in $Ca(OH)_2$ after adding SF. This might suggest that more $Ca(OH)_2$ is involved in subsequent hydration reactions, implying that SF promotes a secondary response between $Ca(OH)_2$ and SiO_2. Besides, after adding SF, the transformation of $Ca(OH)_2$ to a C-S-H gel at about 30° 2θ angles can also be identified, which may further enhance the system's strength [56]. Besides, in the presence of SF, the calcite concentration is found to be increased. This is presumed to be caused by the reason that SF can react with excess $Ca(OH)_2$ to form C-S-H and C-A-S-H gels. This process also enhances carbonation reactions in the atmosphere by providing additional nucleation sites for calcite, especially in the exposed areas where carbonation is more active [57].

3.4. Micromorphological and elemental analysis of hydration products

Fig. 6 presents typical SEM and EDS results of different CFG mixes (0CS, 10CS, 30CS, 70CS, and 30CS10SF) after 28 days of curing. Comparing Fig. 6(a) and (b), it is evident that the 10CS sample produced more flocculated gel material than the 0CS, and the residue of

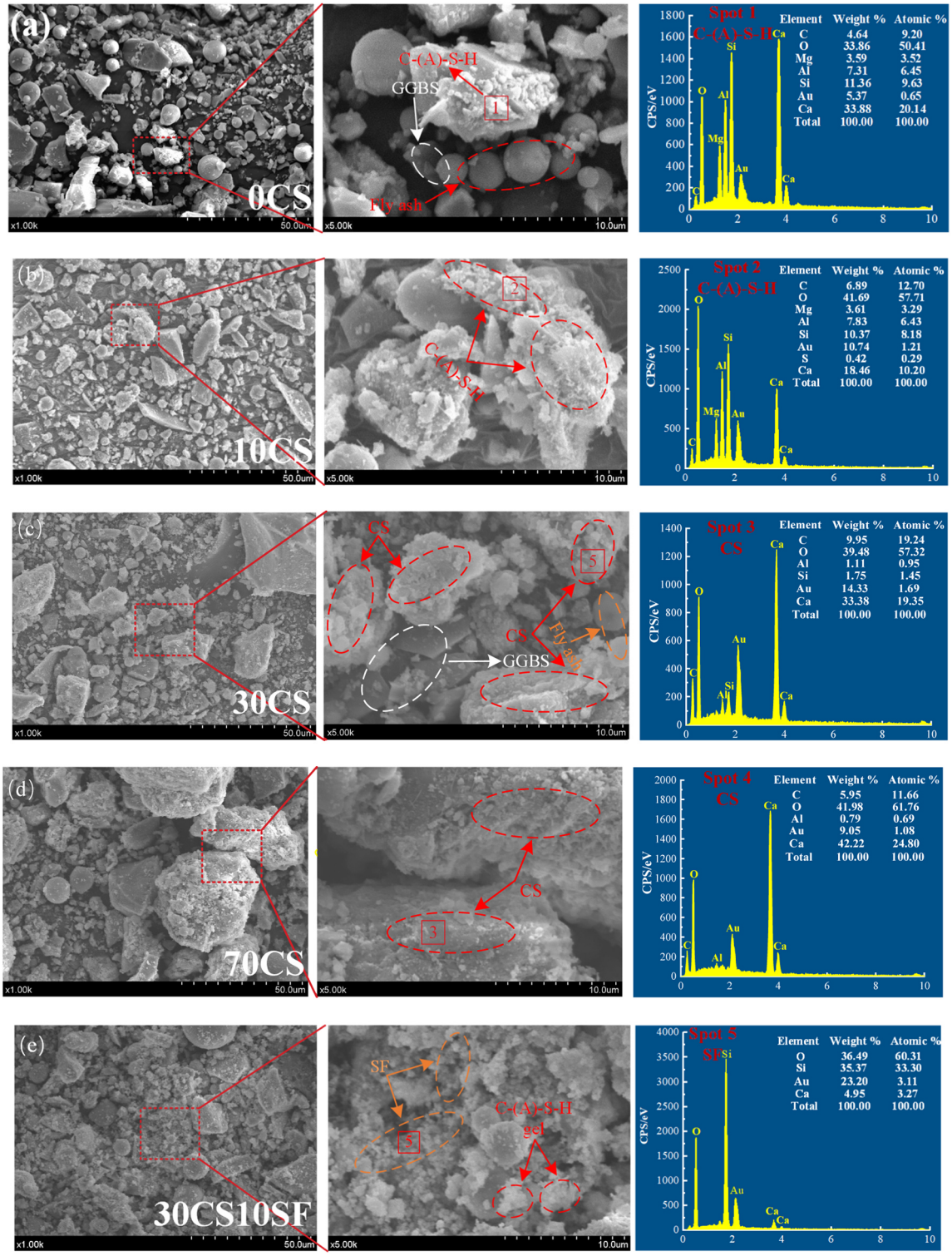


Fig. 6. The SEM and EDS results of the CFG system with different parameters at 28d: (a) 0CS; (b) 10CS; (c) 30CS; (d) 70CS; (e) 30CS10SF.

raw materials, such as FA particles, was scarcely visible. This suggests that the $Ca(OH)_2$ in CS creates an alkaline environment that facilitates hydration, thereby promoting the more complete hydration of FA and GGBS [58]. In Fig. 6(c), residual CS, GGBS, and FA in the system indicate that increased CS content led to more unhydrated particles. A possible explanation for this might be that the increase in CS dosage resulted in a significant increase in alkalinity in the system, which accelerates the hydration reaction, and the

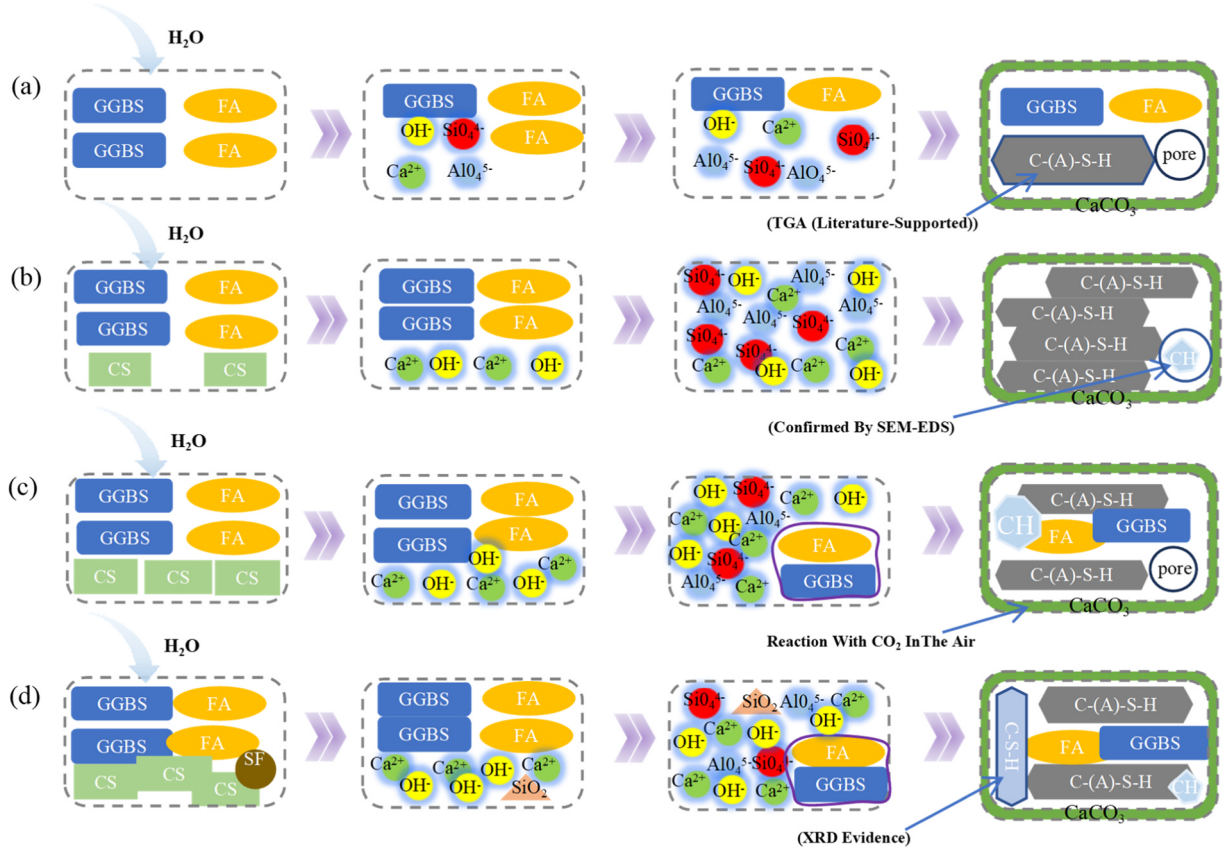


Fig. 7. Speculated hydration mechanism: (a) CFG without CS; (b) CFG with a small amount of CS; (c) CFG with excessive CS; (d) CFG with SF.

rapidly generated gel material may have the trend to the surface of the un-hydrated particles, hindering the continuation of the response [59]. When the CS content reached 70 %, it can be observed in Fig. 6(d) that the residual CS in the system was more pronounced than in low CS dosage samples (refer to Fig. (b) and (c)). As illustrated in Fig. 6(c), it can be seen that the accumulated plate-like products were hexagonal $Ca(OH)_2$ crystals from residual CS combined with the EDS results. These crystals are interspersed with other hydration products and gels, causing the aggregated gel products to become more dispersed, which further increases porosity, weakens the interlayer bonding, prevents the formation of dense structures, and thus hinders the development of mechanical strength [56].

The SEM and EDS results of 30CS10SF are shown in Fig. 6(e). Compared with Fig. 6(c) for 30CS, it is evident that defects like micropores were effectively filled by spherical particles, identified by EDS spot-scanning analysis as SF consisting of Si and O elements. Additionally, the flocculating gel composed of C-S-H is more tightly connected and evenly distributed, with no plate-like CS observed. This suggests that adding SF fills the pores and promotes hydration, transforming the plate-like $Ca(OH)_2$ into a denser flocculating gel [60]. This transformation further binds unreacted particles and effectively fills the pores, resulting in a more compact microstructure and a significant increase in the mechanical strength of the system.

3.5. Discussion on the hydration mechanism of CFG

Based on macroscopic and microscopic analyses of CFG, this study offers some speculative insights into the mechanism of its hydration reactions, combined with chemical formulas (Eqs. (5)–(10)) derived from existing insights and relevant literature. As shown in Fig. 7(a), in the system without CS, GGBS can release alkalis during the hydrolysis process, making the solution weakly alkaline, allowing the decomposition of the aluminum-silica raw materials in GGBS and FA, generating free SiO_4^{4-} and AlO_4^{5-} which combined with the free Ca^{2+} in the system to form a small number of gelation products.

Further, as shown in Fig. 6(a) and (b), Ca^{2+} acts as an essential element for C-(A)-S-H gel formation, and $Ca(OH)_2$ of CS is more efficiently alkali excitation than GGBS, as shown in Eq. 7(b) and Eq. (5), adding a moderate amount of CS, such as in the 10CS system, provided sufficient OH^- to create a favorable alkaline environment. As shown in Eqs. (6) and (7), the OH^- released by CS hydration effectively activated the glassy structures of slag and fly ash, and thus the Al-O and Si-O bonds in the GGBS and FA structures decomposed under OH^- attack, forming silica-oxygen tetrahedra and aluminum-oxygen tetrahedra. These tetrahedra were then combined with Ca^{2+} under alkaline conditions and rebounded to form C-S-H, C-A-H, and C-(A)-S-H, as shown in Eqs. (8)-(10) [52]. As

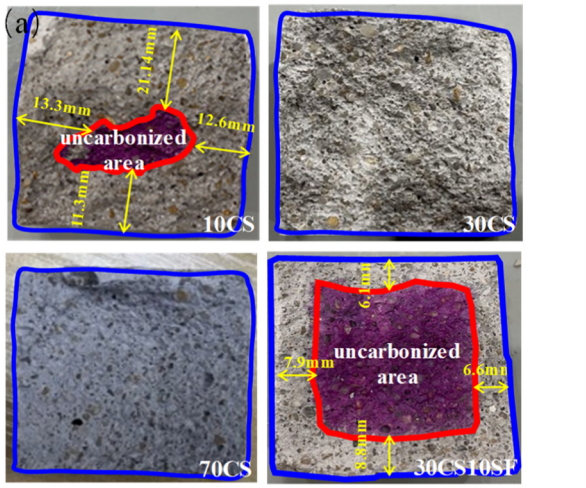


Fig. 8. Performance changes of CFG system after carbonization: (a) carbonization depth of different groups; (b) effect of carbonization on mechanical properties.

shown in the EDS spectrum in Fig. 6(b), the main peaks of Ca, Si, and Al, as well as trace Mg signals, are clearly visible. The atomic ratio of Ca/Si is 1.25, and the Al content is 7.83 wt%. This characteristic is consistent with the definition of C-A-S-H gel, which includes a typical Ca/Si atomic ratio of 1.2–1.8 and an Al content of approximately 5–10 wt% [61]. As the hydration reaction proceeded, the C-(A)-S-H gel continued to grow, attaching to the surface of the unreacted raw material and bonding the dispersed particles into a single unit, thereby imparting high strength to the system. However, when an excessive amount of CS was added to the system, the OH^- concentration became relatively too high, which might cause the rapidly forming hydration products to create a protective layer on the surface of FA and GGBS particles, inhibiting further hydration. Additionally, the excessive CS also led to plate-like $Ca(OH)_2$ accumulation, failing to form sufficiently interconnected gel substances and thus resulting in more micro defects, as shown in Fig. 7(c) [62].

$$Ca(OH)_2 \leftrightarrow Ca^{2+} + 2OH^- \tag{5}$$

$$GGBS + H_2O \rightarrow Ca^{2+} + Mg^{2+} + AlO_4^{5-} + SiO_4^{4-} + OH^- \tag{6}$$

$$FA + H_2O \rightarrow AlO_4^{5-} + SiO_4^{4-} \tag{7}$$

$$SiO_4^{4-} + H_2O + Ca^{2+} \rightarrow C-S-H \tag{8}$$

$$Ca^{2+} + AlO_4^{5-} + H_2O \rightarrow C-A-H \tag{9}$$

$$AlO_4^{5-} + SiO_4^{4-} + H_2O + Ca^{2+} \rightarrow C-A-S-H \tag{10}$$

From previous analyses, it is evident that SF mainly consists of reactive amorphous SiO_2. This allowed it to undergo a gelling reaction with the remaining $Ca(OH)_2$ in the system [58], as shown in Eq. (11). As presented in Fig. 7(d), this reaction transformed the initially loose plate-like $Ca(OH)_2$ structure into a dense C-S-H gelling system. As hydration proceeded, additional C-S-H and C-(A)-S-H gels gradually formed, encapsulating the unreacted material, bonding the dispersed particles into a cohesive whole, and also providing additional nucleation sites to promote carbonation reactions as shown in Eq. (13). This bonding and filling are considered to improve the microporous structure and enhance the matrix's mechanical properties, which is consistent with previous findings.

$$xCa(OH)_2 + SiO_2 + mH_2O \rightarrow xCaO \bullet SiO_2 \bullet (m+x)H_2O \tag{11}$$

3.6. CO_2 sequestration analysis of CFG

Considering that the main component of CS is $Ca(OH)_2$, carbonization tests and microanalysis were conducted to preliminarily verify the CO_2 sequestration capacity of the CFG cementitious system. As shown in Fig. 8(a), after 28 days of accelerated carbonation, a prepared phenolphthalein solution was dropped on the fresh fracture surface after the compressive test, and the uncarbonized portion changed to purplish red. It is evident that the carbonized area of the samples enlarged with the increasing CS content. As shown in Fig. 8(a), it can be found that when the CS content reached 30 % or higher, the samples were completely carbonated. This phenomenon could be attributed to the excessive $Ca(OH)_2$ in the samples with high dosage CS, which promotes the absorption and fixation of external CO_2. Comparatively, in the 10CS group, since the $Ca(OH)_2$ in the system is almost consumed as an alkaline activator. At the

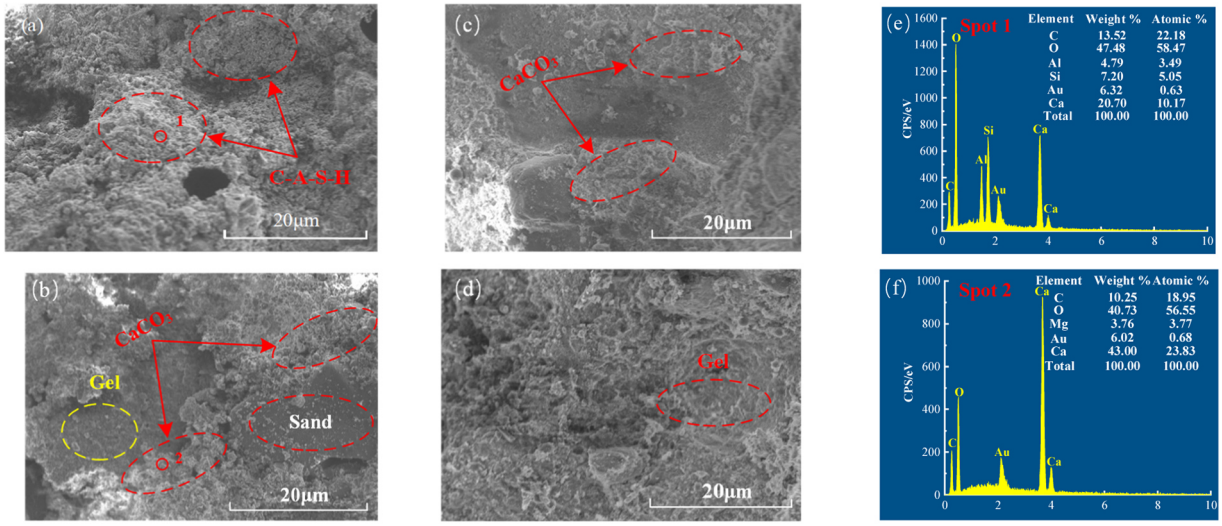


Fig. 9. SEM-EDS characterization of samples after 28 days of carbonization: (a) 10CS; (b) 30CS; (c) 70CS; (d) 30CS10SF; (e) EDS of spot 1; (f) EDS of spot 2.

same time, the absence of excess $Ca(OH)_2$ leads to the formation of a relatively denser microstructure, which prevents further carbonation. Besides, in the 30CS10SF group, the addition of SF notably reduced the carbonized area. This could be caused by the reason that while consuming excess $Ca(OH)_2$, the addition of SF might have increased the density of CFG and comprehensively reduced the penetration depth of CO_2.

After 28 days of carbonation treatment, the changes in compressive strength of mortar specimens with CFG system are shown in Fig. 8(b). The data revealed that when the dosage of CS was 10 %, the compressive strength after carbonation decreased significantly by 40.4 %, which might be because $Ca(OH)_2$ is almost completely consumed and there is not enough $Ca(OH)_2$ to react with external CO_2 in the 10CS cementitious system; further, partial carbonization might have affected the cementing properties of the hydration products [63], thus weakening the overall mechanical performance. However, when the dosage of CS was increased to 30 % and 70 %, the compressive strength started to increase significantly. Especially for the 70CS group, the compressive strength sharply increased by 80.0 % after carbonation. This is attributed to the fact that at higher dosages of CS, $Ca(OH)_2$ is carbonated into finer $CaCO_3$, which significantly improves the microstructure of the mortar, thus improving the mechanical properties. In addition, the compressive strength of the 30CS10SF specimen also increased by 14.8 % to about 35.7 MPa after carbonation, but the degree of increase was smaller than that of the 30CS group. This may be because although the addition of SF can consume most of the $Ca(OH)_2$ remaining in the system, there may be some residual $Ca(OH)_2$, which can react with CO_2 to form $CaCO_3$, which fills the pores and increases the system compactness.

The SEM and EDS images of samples carbonized for 28 days are shown in Fig. 9. From Fig. 9(a) and (b), it can be seen that the structural compactness of the carbonized 30CS sample was better than that of the 10CS sample. In the 10CS sample, it is observed that the gel structure appeared to be looser and was accompanied by larger pores, which could be a critical factor in its reduced compressive strength. Combined with the EDS analysis as shown in Fig. 9(e), it is found that the Ca, Si, Al, and O elements occupied a significant proportion in the EDS spectra, and it is inferred that these elements mainly originated from the C-A-S-H gels. It should be noted that the atomic percentage of Ca element was relatively low at 10.17 %, which implied that the decalcification of the gel may have occurred during the carbonization process, as shown in Eq. (12) [64]. Fig. 9(b) indicates that the 30CS sample had many spherical particles distributed in the voids, which EDS spectral spot-scanning analysis confirms were mainly composed of C, O, and Ca elements, consistent with the atomic ratios of $CaCO_3$ crystals. This suggests that the excessive $Ca(OH)_2$ in the system may have been converted to $CaCO_3$, as shown in Eq. (13) [65]. As shown in Fig. 9(c), the range of gel material in the 70CS samples has decreased and the range of $CaCO_3$ has further increased. This may be because some of the C-(A)-S-H also undergoes a carbonation reaction with CO_2 to produce more $CaCO_3$ [66]. Therefore, in combination with previous carbonization experiments, it may be possible to confirm the high efficiency of CS in carbon sequestration [67]. The microstructure of the 30CS10SF system is shown in Fig. 9(d), where no obvious structural defects were found and the gel was uniformly distributed, which may be attributed to the addition of silica fume. Therefore, it can be known that the addition of silica fume may promote the hydration reaction, resulting in a denser microstructure while also reacting with residual $Ca(OH)_2$ to form more C-S-H, thereby enhancing the material's strength [57].

$$C-S-H+CO_2 \rightarrow SiO_2 \quad gel + CaCO_3 + H_2O \tag{12}$$

$$Ca(OH)_2 + CO_2 \rightarrow CaCO_3 + H_2O \tag{13}$$

Table 3
EC and EE of raw materials.

Raw materials	Embodied CO_2 emission ($kgCO_2/kg$)	Embodied energy (MJ/kg)	Ref.
OPC	0.83	5.75	[63–66]
CS	0.375	1.48	[67]
FA	0.01	0.1	[68,69]
GGBS	0.083	1.6	[69–71]
SF	0.15	0.16	[65,72]

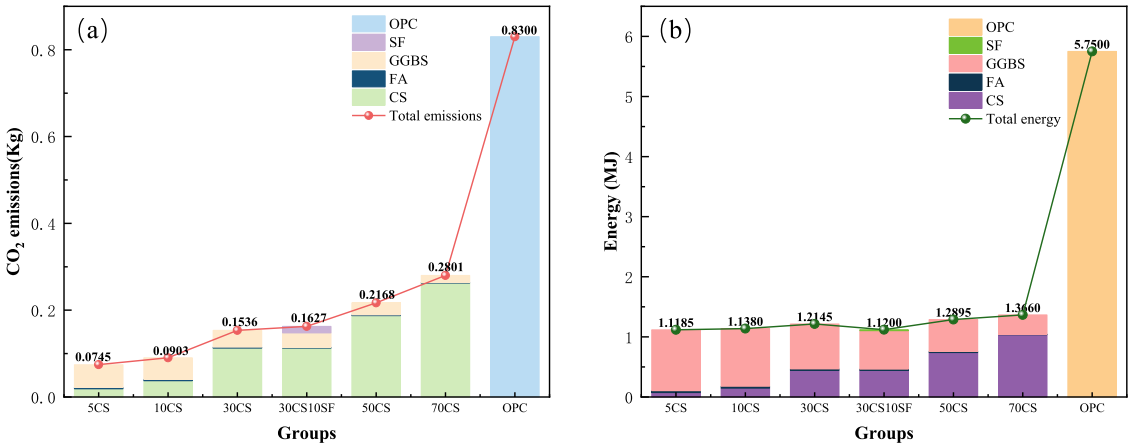


Fig. 10. CO_2 emissions and energy consumption of different pastes: (a) CO_2 emissions of different pastes; (b) energy consumption of different pastes.

3.7. Analysis of the environmental impact of cementitious systems

To assess the environmental impacts, the Life Cycle Assessment (LCA) methodology was utilized to perform carbon and energy assessments on the components of the CFG cementitious systems [68]. The specific evaluation parameters are embedded carbon dioxide emissions (EC) and embedded energy (EE), which are critical parameters for evaluating the environmental friendliness of the designed cementitious materials [69]. The EC calculated here includes the total CO_2 emissions of all raw materials used in the cementitious system, encompassing emissions during transportation, drying, calcination, and sieving. The specific calculation of embodied CO_2 emission is shown in Eq. (14).

$$embodiedCO_2 = \sum_{i=1}^{n} (m_i \times CO_{2i}) \tag{14}$$

Where m_i is the mass per unit volume of a substance; n is the number of components in the mixture; CO_{2i} refers to the embodied CO_2 emissions per unit mass of raw material.

Similar to the calculation of embodied CO_2 emissions, embodied energy consumption is calculated by Eq. (15).

$$embodied_{energy} = \sum_{i=1}^{n} (m_i \times energy_i) \tag{15}$$

Where $Energy_i$ is the embodied energy per unit mass of raw material.

Traditional cement production is notorious for its high energy consumption and significant pollution [62]. In this section, the carbon dioxide emissions and energy consumption of CFG are compared with those of OPC at various stages of the production chain. The calculated data is presented in Table 3.

Based on Eq. (15), and the data in Table 3, the CO_2 emissions and energy consumption for the production of 1 kg of CFG cementitious materials have been calculated. As shown in Fig. 10, all CFG system groups' CO_2 emissions and energy consumption are significantly lower than those of OPC. Notably, the 10CS group with higher mechanical properties performs comparably to cement, with 89.12 % less CO_2 embodied and 80.35 % less energy embodied, highlighting significant environmental advantages. In addition, the data here do not consider the CO_2 sequestration potential of CFG; if the sequestration effect is taken into account, it will have a more positive impact on environmental protection and play a vital role in promoting low-carbon development.

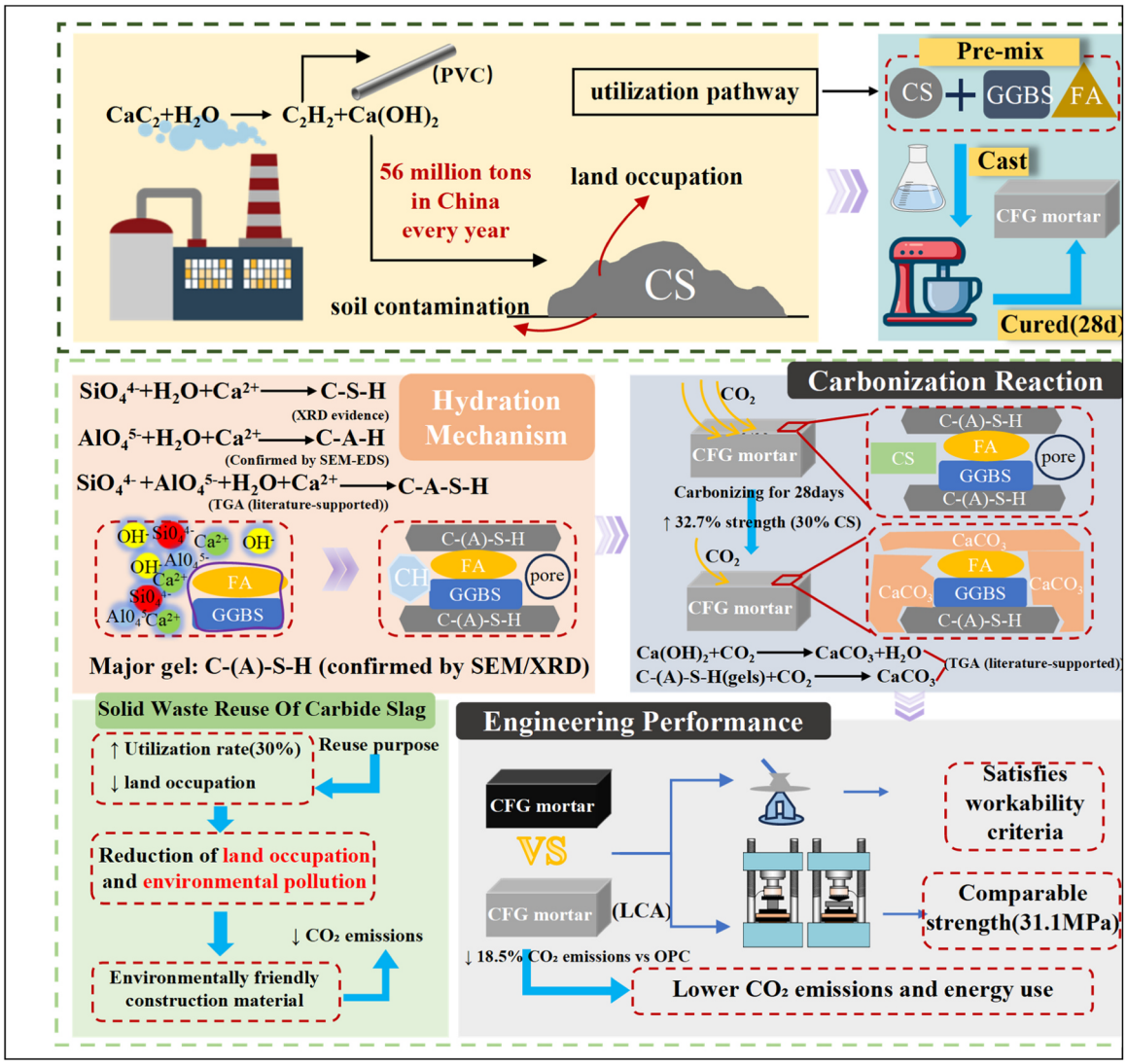


Fig. 11. Performance improvement and environmental friendliness of CFG.

3.8. Performance improvement mechanism of CFG

A schematic diagram of the performance improvement and environmental friendliness of CFG is shown in Fig. 11. The traditional ways of treating CS harm the environment, so it is necessary to find a scientific and efficient method. Attempts to prepare cementitious materials using CS, FA, and GGBS have yielded some exciting results. By testing the working performance and strength of CFG and combining it with the LCA environmental assessment method, it can be found that CFG not only has a particular engineering application prospect but is also conducive to the reuse of CS, which is an environmentally friendly construction material.

CS increases the system's alkalinity and provides calcium, which facilitates the formation of gel substances, enhancing the material's structure. However, high CS content leads to an accumulation of $Ca(OH)_2$, increasing porosity. Excessive CS also allows the cementitious mortar to absorb CO_2, enhancing its strength. The CFG system also demonstrates excellent carbon capture capabilities and attendant performance enhancements.

4. Conclusions

This study designs a low-carbon cementitious material CFG based on solid wastes CS, FA, and GGBS. Through a series of macroscopic mechanical and carbonation tests as well as microscopic analysis, the feasibility of CFG is evaluated. The influential rules of crucial factors such as CS dosage on the performance and carbon sequestration of CFG, as well as the corresponding hydration mechanisms, are discussed. In addition, the value of CFG in terms of environmental protection is evaluated. The main findings of this

study are summarized as follows:

(1) Through the tests of working and mechanical properties, it can be found that CFG has the potential to replace cement as a low-carbon cementitious material. The initial setting time of CFG ranged from 2.4 to 7.1 h, and the final setting time varied between 3.4 and 8.9 h at different dosages of CS, meeting the OPC's setting time requirement. Both the flexural and compressive strengths of CFG showed an increasing and then decreasing trend with the increase of CS dosage. When the CS dosage was 10 %, the flexural and compressive strengths at 28 days reached the maximum value, 7.7 and 29.2 MPa, respectively. This observation provides an essential basis for future practical engineering construction applications.
(2) Microanalysis by SEM-EDS and XRD shows that the CS can act as an alkaline exciter, effectively activating the FA and GGBS, separating the silica-aluminum vitreous, and restructuring them with free Ca^{2+} to produce gel substances. However, an excessive amount of CS (30 % dosage and above) caused $Ca(OH)_2$ accumulation in CFG, which reduced the microstructural densification and was unfavorable to the system's strength. The addition of silica fume can consume the excess $Ca(OH)_2$, e.g., adding 10 % SF in the group of 30CS improved the compressive strength by 54 % from 20.2 MPa to 31.1 MPa.
(3) CFG can play a role in absorbing CO_2. With the increase in the amount of CS, the degree of carbonization of CFG was higher. Especially when the amount of CS reaches 30 % and above, the specimen is almost completely carbonized. This was probably because there was residual $Ca(OH)_2$ in the excessive CS system, which can react with CO_2 to form $CaCO_3$; this not only had the effect of CO_2 sequestration but also had a specific contribution to the strength enhancement. In the specimens with 30 % and 70 % CS dosage, the compressive strength after carbonation increased by 32.7 % as 35.7 MPa and 80 % as 19.8 MPa, respectively. The discovery of this carbon sequestration property may make CFG highly valuable in environmental protection.
(4) CFG can be a viable alternative to OPC and significantly reduce CO_2 emissions and energy consumption. The 10CS group, with performance similar to China's 32.5-grade cement, reduced CO_2 emissions by up to 89.12 % and energy consumption by 80.35 %. In addition, the carbon sequestration and the performance enhancement capacity of the CFG system enrich its further environmental advantages.

CRediT authorship contribution statement

Yulong Zheng: Writing – review & editing, Resources. **Jingquan Wang:** Validation, Supervision. **Chang Liu:** Investigation, Formal analysis. **Xingpei Yan:** Investigation, Conceptualization. **Haozhe Pan:** Writing – original draft, Visualization. **Guiyu Zhang:** Data curation, Conceptualization. **Stuart T. Wagland:** Supervision. **Liang Cheng:** Methodology, Conceptualization.

Declaration of Competing Interest

The authors declare that they have no known competing financial interests or personal relationships that could have appeared to influence the work reported in this paper.

Acknowledgements

This work was financially supported by the National Natural Science Foundation of China (Nos. 52108147 and 52341802) and the Senior Talent Foundation of Jiangsu University (No. 20JDG19).

Data availability

Data will be made available on request.

References

[1] J. Sun, W.Q. Liu, Y.C. Hu, J.Q. Wu, M.K. Li, X.W. Yang, W.Y. Wang, M.H. Xu, Enhanced performance of extruded-spheronized carbide slag pellets for high temperature CO_2 capture, Chem. Eng. J. 285 (2016) 293–303, https://doi.org/10.1016/j.cej.2015.10.026.
[2] Y.X. Shi, Q.X. Zhao, C.H. Xue, Y.L. Jia, W.C. Guo, Y.Y. Zhang, Y.X. Qiu, Preparation and curing method of red mud-calcium carbide slag synergistically activated Fly ash-ground granulated blast furnace slag based eco-friendly geopolymer, Cem. Concr. Compos 139 (2023) 104999, https://doi.org/10.1016/j.cemconcomp.2023.104999.
[3] J. Yang, L.P. Ma, H.P. Liu, Y. Wei, B. Keomounlath, Q.X. Dai, Thermodynamics and kinetics analysis of Ca-looping for CO_2 capture: application of carbide slag, Fuel 242 (2019) 1–11, https://doi.org/10.1016/j.fuel.2019.01.018.
[4] W.C. Guo, Z.Y. Zhang, Y.Y. Bai, G.Q. Zhao, Z.H. Sang, Q.X. Zhao, Development and characterization of a new multi-strength level binder system using soda residue-carbide slag as composite activator, Constr. Build. Mater. 291 (2021) 123367, https://doi.org/10.1016/j.conbuildmat.2021.123367.
[5] M.Y. Li, Q.X. Zhao, C.S. Li, H.M. Pan, Optimization design and mechanical properties of multi-component ecological gelling materials, J. Clean. Prod. 443 (2024) 140970, https://doi.org/10.1016/j.jclepro.2024.140970.
[6] J. Liu, C.W. Yan, J. Zhang, J.Q. Li, J.H. Zhao, X.W. Shen, F. Cao, G.C. Zhang, X.D. Meng, Characteristics of AC impedance and pore structure in solid waste-based cementitious materials with different water-to-binder ratios, Constr. Build. Mater. 467 (2025) 140342, https://doi.org/10.1016/j.conbuildmat.2025.140342.
[7] B. Guo, T.X. Zhao, F. Sha, F. Zhang, Q. Li, J. Zhao, J.B. Zhang, Synthesis of vaterite $CaCO_3$ micro-spheres by carbide slag and a novel CO_2-storage material, J. CO_2 Util. 18 (2017) 23–29, https://doi.org/10.1016/j.jcou.2017.01.004.
[8] C. Phetchuay, S. Horpibulsuk, C. Suksiripattanapong, A. Chinkulkijniwat, A. Arulrajah, M.M. Disfani, Calcium carbide residue: alkaline activator for clay-Fly ash geopolymer, Constr. Build. Mater. 69 (2014) 285–294, https://doi.org/10.1016/j.conbuildmat.2014.07.018.
[9] S.M. Wu, Y.J. Li, J.L. Zhao, C.M. Lu, Z.Y. Wang, Simultaneous CO_2/SO_2 adsorption performance of carbide slag in Adsorption/Desorption cycles, Can. J. Chem. Eng. 94 (1) (2016) 33–40, https://doi.org/10.1002/cjce.22369.

[10] G. Montes-Hernandez, R. Pérez-López, F. Renard, J.M. Nieto, L. Charlet, Mineral sequestration of CO_2 by aqueous carbonation of coal combustion Fly-ash, J. Hazard. Mater. 161 (2-3) (2009) 1347–1354, https://doi.org/10.1016/j.jhazmat.2008.04.104.
[11] M.A. Karim, S. Nasir, S.A. Rachman, Novia, Reduction of Iron (II) Ions in Synthetic Acidic Wastewater Containing Ferro Sulphate Using Calcium Carbide Residu, 11th Regional Conference on Chemical Engineering, 2019, p. 020025. https://doi.org/10.1063/1.5095003.
[12] W.X. Li, Y. Huang, T. Wang, M.X. Fang, Y. Li, Preparation of calcium carbonate nanoparticles from waste carbide slag based on CO_2 mineralization, J. Clean. Prod. 363 (2022) 132463, https://doi.org/10.1016/j.jclepro.2022.132463.
[13] H. Ma, X. Feng, Y.B. Yang, Z.F. Zhang, C. Deng, Preparation of feed grade calcium formate from calcium carbide residue, Clean. Technol. Environ. Policy 18 (6) (2016) 1905–1915, https://doi.org/10.1007/s10098-016-1119-x.
[14] L. Shao, L. Ma, J. Yang, Q. Dai, L. Xie, Y. Luo, L. Zeng, Re-utilization status of carbide slag (in chinese), Mod. Chem. Ind. 44 (3) (2024) 79–83, https://doi.org/10.16606/j.cnki.issn0253-4320.2024.03.016.
[15] R.Q. Wang, G.D. Li, C.Y. Li, Y.P. Huo, T. Wang, P. Hou, Z. Gong, Study on the design method of multi-component industrial solid waste low carbon cementitious material with cement as the activator, Case Stud. Constr. Mater. 21 (2024) e03478, https://doi.org/10.1016/j.cscm.2024.e03478.
[16] F. Avet, K. Scrivener, Investigation of the calcined kaolinite content on the hydration of limestone calcined clay cement (LC^3), Cem. Concr. Res. 107 (2018) 124–135, https://doi.org/10.1016/j.cemconres.2018.02.016.
[17] Y. Wan, Y.X. Guo, C.Q. Li, X.C. Li, G.R. Feng, Synthesis use of coal gasification slag to prepare belite sulphoaluminate cementitious material and its hydration characteristics study, Constr. Build. Mater. 467 (2025) 140370, https://doi.org/10.1016/j.conbuildmat.2025.140370.
[18] M.J. Nazir, G.L. Li, M.M. Nazir, F. Zulfiqar, K.H.M. Siddique, B. Iqbal, D.L. Du, Harnessing soil carbon sequestration to address climate change challenges in agriculture, Soil Tillage Res. 237 (2024) 105959, https://doi.org/10.1016/j.still.2023.105959.
[19] D. Parthiban, D.S. Vijayan, E. Koda, M.D. Vaverkova, K. Piechowicz, P. Osinski, B.V. Duc, Role of industrial based precursors in the stabilization of weak soils with geopolymer - a review, Case Stud. Constr. Mater. 16 (2022) e00886, https://doi.org/10.1016/j.cscm.2022.e00886.
[20] F.A. Ababneh, A.I. Alakhras, M. Heikal, S.M. Ibrahim, Stabilization of lead bearing sludge by utilization in Fly ash-slag based geopolymer, Constr. Build. Mater. 227 (2019) 116694, https://doi.org/10.1016/j.conbuildmat.2019.116694.
[21] J.M. Li, L.W. Guo, J.Y. Zhang, Y. Li, L. Ma, K. Wang, Study on the synergistic hydration mechanism of granulated blast furnace slag-carbide slag-based cementitious materials and the properties of full-solid waste backfill materials, Sci. Rep. 15 (1) (2025) 1947, https://doi.org/10.1038/s41598-025-86509-7.
[22] W.Y. Qi, G. Duan, Y.J. Han, Q.X. Zhao, Y.L. Huang, W.H. Zhu, H.T. Pang, J.H. Zhang, Comparison of mechanical properties and microstructure of GGBS-based cementitious materials activated by different combined alkaline wastes, Constr. Build. Mater. 422 (2024) 135784, https://doi.org/10.1016/j.conbuildmat.2024.135784.
[23] W.T. Li, Y.L. Yi, Use of carbide slag from acetylene industry for activation of ground granulated blast-furnace slag, Constr. Build. Mater. 238 (2020) 117713, https://doi.org/10.1016/j.conbuildmat.2019.117713.
[24] Y.B. Feng, F. Li, W.Y. Qi, Q.S. Ren, W.Y. Qi, G. Duan, K.L. Zheng, Y.J. Han, H.T. Pang, Mechanical properties and microstructure of iron tailings cemented paste backfills using carbide Slag-Activated ground granulated Blast-Furnace slag as alternative binder, Minerals 12 (2022) 1549, https://doi.org/10.3390/min12121549.
[25] S. Dueramae, W. Tangchirapat, P. Sukontasukkul, P. Chindaprasirt, C. Jaturapitakkul, Investigation of compressive strength and microstructures of activated cement free binder from Fly ash - calcium carbide residue mixture, J. Mater. Res. Technol. 8 (2019) 4757–4765, https://doi.org/10.1016/j.jmrt.2019.08.022.
[26] C. Namarak, P. Satching, W. Tangchirapat, C. Jaturapitakkul, Improving the compressive strength of mortar from a binder of Fly ash-calcium carbide residue, Constr. Build. Mater. 147 (2017) 713–719, https://doi.org/10.1016/j.conbuildmat.2017.04.167.
[27] P. Julphunthong, P. Joyklad, P. Manprom, T. Chompoorat, M.T. Palou, T. Suriwong, Evaluation of calcium carbide residue and Fly ash as sustainable binders for environmentally friendly loess soil stabilization, Sci. Rep. 14 (1) (2024) 671, https://doi.org/10.1038/s41598-024-51326-x.
[28] C. Jaturapitakkul, B. Roongreung, Cementing material from calcium carbide residue-rice husk ash, J. Mater. Civ. Eng. 15 (5) (2003) 470–475, https://doi.org/10.1061/(ASCE)0899-1561(2003)15:5(470).
[29] C. Rattanashotinunt, P. Thairit, W. Tangchirapat, C. Jaturapitakkul, Use of calcium carbide residue and bagasse ash mixtures as a new cementitious material in concrete, Mater. Des. 46 (2013) 106–111, https://doi.org/10.1016/j.matdes.2012.10.028.
[30] L.L. Zhang, Y.S. Ji, G.D. Huang, J. Li, Y.J. Hu, Modification and enhancement of mechanical properties of dehydrated cement paste using ground granulated blast-furnace slag, Constr. Build. Mater. 164 (2018) 525–534, https://doi.org/10.1016/j.conbuildmat.2017.12.232.
[31] Y. Lou, K. Khan, M.N. Amin, W. Ahmad, A.F. Deifalla, A. Ahmad, Performance characteristics of cementitious composites modified with silica fume: a systematic review, Case Stud. Constr. Mater. 18 (2023) e01753, https://doi.org/10.1016/j.cscm.2022.e01753.
[32] H.S. Wong, H.A. Razak, Efficiency of calcined kaolin and silica fume as cement replacement material for strength performance, Cem. Concr. Res. 35 (4) (2005) 696–702, https://doi.org/10.1016/j.cemconres.2004.05.051.
[33] X.Y. Li, K.P. Zhao, Z.T. Li, X.B. Li, K. Peng, All-solid-waste-derived CaO-based sorbents for simultaneously enhanced calcium looping CO_2 capture and thermochemical energy storage, J. Clean. Prod. 470 (2024) 143270, https://doi.org/10.1016/j.jclepro.2024.143270.
[34] Q. Zhang, P. Feng, X.Y. Shen, Y.W. Zhang, S.Y. Bian, T.C. Ling, Assessment method of carbonation degree and activity of a wide range of calcium/magnesium containing solids, J. Clean. Prod. 467 (2024) 143009, https://doi.org/10.1016/j.jclepro.2024.143009.
[35] S.J. Wang, X. Lin, Y. Zhang, C.Q. Wang, A review of utilizing carbide slag to sequestrate carbon dioxide by mineral carbonation: mechanisms, processes, and value-added products, Fuel 384 (2025) 134041, https://doi.org/10.1016/j.fuel.2024.134041.
[36] N. Makaratat, C. Jaturapitakkul, C. Namarak, V. Sata, Effects of binder and CaCl2 contents on the strength of calcium carbide residue-Fly ash concrete, Cem. Concr. Compos. 33 (2011) 436–443, https://doi.org/10.1016/j.cemconcomp.2010.12.004.
[37] Y. Wang, Y. Hu, X. He, Y. Su, B. Strnadel, W. Miao, Hydration and compressive strength of supersulfated cement with low-activity high alumina ferronickel slag, Cem. Concr. Compos. 136 (2023) 104892, https://doi.org/10.1016/j.cemconcomp.2022.104892.
[38] L.Z. Guo, J.H. Liu, M. Zhou, S.H. An, Effect of an alkali activators on the compressive strength and reaction mechanism of coal gangue-slag-Fly ash geopolymer grouting materials, Constr. Build. Mater. 426 (2024) 136012, https://doi.org/10.1016/j.conbuildmat.2024.136012.
[39] P. Mounanga, M.I.A. Khokhar, R. El Hachem, A. Loukili, Improvement of the early-age reactivity of Fly ash and blast furnace slag cementitious systems using limestone filler, Mater. Struct. 44 (2) (2011) 437–453, https://doi.org/10.1617/s11527-010-9637-1.
[40] C.L. Hu, Z.J. Li, Property investigation of individual phases in cementitious composites containing silica fume and Fly ash, Cem. Concr. Compos. 57 (2015) 17–26, https://doi.org/10.1016/j.cemconcomp.2014.11.011.
[41] GB/T 50082-2009, Standard Test Methods for Long-Term and Durability Properties of Ordinary Concrete, 2009(in chinese).
[42] W. Al Makhadmeh, A. Soliman, Effect of activator nature on property development of alkali-activated slag binders, J. Sustain. Cem. Based Mater. 10 (4) (2020) 240–256, https://doi.org/10.1080/21650373.2020.1833256.
[43] X. Ji, Z.J. Wang, X.F. Wang, X. Zhao, H.B. Zhang, T.H. Zhang, Microstructures and properties of alkali-activated slags with composite activator: effects of Na_2O equivalents, J. Clean. Prod. 450 (2024) 141754, https://doi.org/10.1016/j.jclepro.2024.141754.
[44] X.G. Sun, J. Liu, J.P. Qiu, P.Q. Wu, Y.Q. Zhao, Alkali activation of blast furnace slag using a carbonate-calcium carbide residue alkaline mixture to prepare cemented paste backfill, Constr. Build. Mater. 320 (2022) 126234, https://doi.org/10.1016/j.conbuildmat.2021.126234.
[45] Y.Q. Zhao, X.W. Gu, X.C. Xu, Z.L. Zhang, Using calcium carbide residue to prepare ecological alkali activated slag composites: effect of anion type, Ceram. Int. 49 (15) (2023) 25092–25104, https://doi.org/10.1016/j.ceramint.2023.05.039.
[46] Y.L. Zhang, X.M. Liu, Y.T. Xu, B.W. Tang, Y.G. Wang, E. Mukiza, Synergic effects of electrolytic manganese residue-red mud-carbide slag on the road base strength and durability properties, Constr. Build. Mater. 220 (2019) 364–374, https://doi.org/10.1016/j.conbuildmat.2019.06.009.
[47] O. Simsek, H.Y. Aruntas, I. Demir, H. Yaprak, S. Yazicioglu, Investigation of the effect of seawater and sulfate on the properties of cementitious composites containing silica fume, Silicon 14 (2) (2022) 663–675, https://doi.org/10.1007/s12633-021-01052-0.
[48] X.Y. Xu, X.J. Lin, X.X. Pan, T. Ji, Y.N. Liang, H.R. Zhang, Influence of silica fume on the setting time and mechanical properties of a new magnesium phosphate cement, Constr. Build. Mater. 235 (2020) 117544, https://doi.org/10.1016/j.conbuildmat.2019.117544.

[49] H.W. Li, R. Wang, M.W. Wei, N.Z. Lei, T.B. Wei, F. Liu, Characteristics of carbide-slag-activated GGBS-Fly ash materials: strength, hydration mechanism, microstructure, and sustainability, Constr. Build. Mater. 422 (2024) 135796, https://doi.org/10.1016/j.conbuildmat.2024.135796.
[50] W.T. Li, Y.L. Yi, Use of carbide slag from acetylene industry for activation of ground granulated blast-furnace slag, Constr. Build. Mater. 238 (2020) 117713, https://doi.org/10.1016/j.conbuildmat.2019.117713.
[51] M.R. Ahmad, B. Chen, Effect of silica fume and basalt fiber on the mechanical properties and microstructure of magnesium phosphate cement (MPC) mortar, Constr. Build. Mater. 190 (2018) 466–478, https://doi.org/10.1016/j.conbuildmat.2018.09.143.
[52] A. Fernández-Jiménez, A. Palomo, Composition and microstructure of alkali activated Fly ash binder: effect of the activator, Cem. Concr. Res. 35 (2005) 1984–1992, https://doi.org/10.1016/j.cemconres.2005.03.003.
[53] P. Julphunthong, P. Joyklad, P. Manprom, T. Chompoorat, M.-T. Palou, T. Suriwong, Evaluation of calcium carbide residue and Fly ash as sustainable binders for environmentally friendly loess soil stabilization, Sci. Rep. 14 (2024) 671, https://doi.org/10.1038/s41598-024-51326-x.
[54] K. Wang, H. Zheng, S. Li, Y. Sun, H. Ba, J. Ma, Study on carbonation behavior and carbon footprint of steel slag-calcium carbide slag-desulfurization gypsum composite system, Sci. Rep. 15 (2025) 15199, https://doi.org/10.1038/s41598-025-99803-1.
[55] N. Zhang, H. Li, X. Liu, Hydration mechanism and leaching behavior of bauxite-calcination-method red mud-coal gangue based cementitious materials, J. Hazard. Mater. 314 (2016) 172–180, https://doi.org/10.1016/j.jhazmat.2016.04.040.
[56] R.T. Kou, M.Z. Guo, L. Han, J.S. Li, B. Li, H.Q. Chu, L.H. Jiang, L. Wang, W.Z. Jin, C.S. Poon, Recycling sediment, calcium carbide slag and ground granulated blast-furnace slag into novel and sustainable cementitious binder for production of eco-friendly mortar, Constr. Build. Mater. 305 (2021) 124772, https://doi.org/10.1016/j.conbuildmat.2021.124772.
[57] Y.L. Huo, J.G. Huang, D. Lu, X.Y. Han, H.Y. Sun, T.A. Liu, J.H. Wang, F. Wang, P. Tan, M. Wang, J.Y. Zhou, Y.Z. Yang, Durability of alkali-activated slag concrete incorporating silica fume and rice husk ash, J. Build. Eng. 78 (2023) 107637, https://doi.org/10.1016/j.jobe.2023.107637.
[58] D.P. Bentz, Modeling the influence of limestone filler on cement hydration using CEMHYD3D, Cem. Concr. Compos 28 (2) (2006) 124–129, https://doi.org/10.1016/j.cemconcomp.2005.10.006.
[59] G. Jian, W. Xiaolei, L. Jun, L. Yancang, L. Libo, Experimental study on preparation of baking-free bricks from blast furnace slag, N. Build. Mater. /Xinxing Jianzhu Cailiao 49 (2022) 165–168, https://doi.org/10.3969/j.issn.1001-702X.2022.11.034.
[60] T. Schade, F. Bellmann, B. Middendorf, Quantitative analysis of C-(K)-A-S-H-amount and hydrotalcite phase content in finely ground highly alkali-activated slag/silica fume blended cementitious material, Cem. Concr. Res. 153 (2022) 106706, https://doi.org/10.1016/j.cemconres.2021.106706.
[61] X. Gao, X. Yao, T. Yang, S. Zhou, H. Wei, Z. Zhang, Calcium carbide residue as auxiliary activator for one-part sodium carbonate-activated slag cements: compressive strength, phase assemblage and environmental benefits, Constr. Build. Mater. 308 (2021) 125015, https://doi.org/10.1016/j.conbuildmat.2021.125015.
[62] F. Puertas, S. Martínez-Ramírez, S. Alonso, T. Vázquez, Alkali-activated Fly ash/slag cement -: strength behaviour and hydration products, Cem. Concr. Res. 30 (10) (2000) 1625–1632, https://doi.org/10.1016/S0008-8846(00)00298-2.
[63] Q. Zhang, P. Feng, X.Y. Shen, Y.X. Cai, H.R. Zhen, Z.C. Liu, Comparative analysis of carbonation strengthening mechanisms in full solid waste materials: steel slag vs. Carbide slag, Cem. Concr. Compos 157 (2025) 105927, https://doi.org/10.1016/j.cemconcomp.2025.105927.
[64] S. von Greve-Dierfeld, B. Lothenbach, A. Vollpracht, B. Wu, B. Huet, C. Andrade, C. Medina, C. Thiel, E. Gruyaert, H. Vanoutrive, I.F. Saéz del Bosque, I. Ignjatovic, J. Elsen, J.L. Provis, K. Scrivener, K.-C. Thienel, K. Sideris, M. Zajac, N. Alderete, Ö. Cizer, P. Van den Heede, R.D. Hooton, S. Kamali-Bernard, S. A. Bernal, Z. Zhao, Z. Shi, N. De Belie, Understanding the carbonation of concrete with supplementary cementitious materials: a critical review by RILEM TC 281-CCC, Mater. Struct. 53 (2020) 136, https://doi.org/10.1617/s11527-020-01558-w.
[65] I. Baur, C. Ludwig, C.A. Johnson, The leaching behavior of cement stabilized air pollution control residues: a comparison of field and laboratory investigations, Environ. Sci. Technol. 35 (13) (2001) 2817–2822, https://doi.org/10.1021/es000243r.
[66] P.Y. Chen, C.J. Wang, Y.H. Wang, J.K. Xie, X. Shen, C. Wang, J.L. Wang, Pre-carbonation of calcium carbide slag for the preparation of eco-friendly mortars, Constr. Build. Mater. 399 (2023) 132541, https://doi.org/10.1016/j.conbuildmat.2023.132541.
[67] Z.H. Ma, H.Q. Liao, F.Q. Cheng, Synergistic mechanisms of steelmaking slag coupled with carbide slag for CO_2 mineralization, Int. J. Greenh. Gas. Control 105 (2021) 103229, https://doi.org/10.1016/j.ijggc.2020.103229.
[68] M. Manjunatha, S. Preethi, Malingaraya, H.G. Mounika, K.N. Niveditha, Ravi, Life cycle assessment (LCA) of concrete prepared with sustainable cement-based materials, Mater. Today. Proc. 47 (2021) 3637–3644, https://doi.org/10.1016/j.matpr.2021.01.248.
[69] Y.H. Zhao, S. Wang, J.Q. Yang, Z.H. Zhang, Y. Liu, Input-output analysis of carbon emissions embodied in China-Japan trade, Appl. Econ. 48 (16) (2016) 1515–1529, https://doi.org/10.1080/00036846.2015.1102845.



https://dspace.org/

High-dosage carbide slag-based cementitious material: workability, mechanical strength, and carbonation behavior with the performance enhancement

Zheng, Yulong; Liu, Chang; Wang, Jingquan; Pan, Haozhe; Yan, Xingpei ...

2025-12-01
Elsevier
https://doi.org/10.1016/j.cscm.2025.e05145
Zheng Y, Liu C, Wang J, et al., (2025) High-dosage carbide slag-based cementitious material: workability, mechanical strength, and carbonation behavior with the performance enhancement. Case Studies in Construction Materials, Volume 23, December 2025, Article number e05145

Downloaded from a DSpace repository. https://dspace.org/